

OPEN ACCESS

EDITED BY
Itamar Ronen,
Brighton and Sussex Medical School,
United Kingdom

REVIEWED BY
Cesar Caballero-Gaudes,
Basque Center on Cognition, Brain and
Language, Spain
Thomas Lindner,
University of Hamburg, Germany

*CORRESPONDENCE
Ke Zhang

☑ ke.zhang@uni-heidelberg.de

RECEIVED 28 November 2024 ACCEPTED 26 September 2025 PUBLISHED 10 October 2025

CITATION

Zhang K, Triphan SMF, Wielpütz MO, Jende J, Sleight E, Ziener CH, Ladd ME, Schlemmer H-P, Kauczor H-U, Sedlaczek O and Kurz FT (2025) Correlation of breathing task derived cerebrovascular reactivity with baseline CBF, OEF and CMRO₂. Front. Neurol. 16:1534844. doi: 10.3389/fneur.2025.1534844

COPYRIGHT

© 2025 Zhang, Triphan, Wielpütz, Jende, Sleight, Ziener, Ladd, Schlemmer, Kauczor, Sedlaczek and Kurz. This is an open-access article distributed under the terms of the Creative Commons Attribution License (CC BY). The use, distribution or reproduction in other forums is permitted, provided the original author(s) and the copyright owner(s) are credited and that the original publication in this journal is cited, in accordance with accepted academic practice. No use, distribution or reproduction is permitted which does not comply with these terms.

Correlation of breathing task derived cerebrovascular reactivity with baseline CBF, OEF and CMRO₂

Ke Zhang^{1*}, Simon M. F. Triphan¹, Mark O. Wielpütz^{1,2}, Johan Jende³, Emilie Sleight⁴, Christian Herbert Ziener³, Mark E. Ladd⁵, Heinz-Peter Schlemmer³, Hans-Ulrich Kauczor¹, Oliver Sedlaczek^{1,3} and Felix T. Kurz^{3,6}

¹Department of Diagnostic and Interventional Radiology, Heidelberg University Hospital, Heidelberg, Germany, ²Department of Diagnostic Radiology and Neuroradiology, University Medicine Greifswald, Greifswald, Germany, ³Division of Radiology, German Cancer Research Center, Heidelberg, Germany, ⁴CIBM Center for Biomedical Imaging, Geneva, Switzerland, ⁵Division of Medical Physics in Radiology, German Cancer Research Center, Heidelberg, Germany, ⁶Division of Neuroradiology, Geneva University Hospitals, Geneva, Switzerland

Rationale and objectives: Only a few studies examined the correlation between cerebrovascular reactivity (CVR) and other physiological parameters such as cerebral blood flow (CBF), oxygen extraction fraction (OEF) and cerebral metabolic rate of oxygen (CMRO₂). In this study, these baseline parameters were measured using 3D MRI with whole brain coverage for the investigation of global and regional correlation between each other to enhance understanding of brain function and improve tumor diagnosis.

Materials and methods: All measurement were performed at 3 T. CVR was derived from a breath-holding task. Baseline CBF was measured by pseudocontinuous arterial spin labeling. Baseline OEF was measured with a gradient-echo sampling of spin-echo pulse sequence. T1 weighted anatomical image (T1W) was measured using MPRAGE sequence. CVR was calculated using customized written programs. CBF was quantified by using ASLtbx. For OEF analysis, a feedforward artificial neural network was used. CMRO₂ was calculated based on smoothed and normalized CBF and OEF. General linear regression analysis was used to examine the relations between CVR and other parameters in five lobes of gray matter including frontal, parietal, temporal, occipital and insula lobes in individual healthy subjects. Spearman correlation was performed to check the regional correlations in an Automated Anatomical Labeling (AAL) atlas

Results: Fifteen healthy volunteers and five patients with brain tumors were included. In the healthy subjects, five lobes had a positive correlation between CBF and CVR (p < 0.05). Similarly, in five lobes positive correlations between CMRO₂ and CVR were found (p < 0.05), as well as significant inter- and intrasubject correlations (p < 0.001). However, there were no significant correlations between OEF and other parameters.

Conclusion: Our findings demonstrate that CVR is strongly associated with CBF and CMRO₂ at both global and regional levels in healthy brains, but not with OEF. These results provide new insight into the complex interplay between vascular reactivity, perfusion, and metabolism and underscore the potential of combined CVR-CBF-CMRO₂ imaging for assessing brain health and pathology.

KEYWORDS

cerebrovascular reactivity, cerebral blood flow, oxygen extraction fraction, cerebral metabolic rate of oxygen, correlationship

Introduction

Cerebrovascular reactivity (CVR) is an index of the brain vessels' dilatory capacity, and is typically measured using hypercapnic gas inhalation or breath-holding as a vasoactive challenge (1–3). Research indicates that the baseline vascular state is associated with CVR. During task-induced and resting states, changes in CVR were shown to be modulated by the vascular and metabolic baseline states (4–9). The vascular and metabolic baseline states includes cerebral blood flow (CBF), oxygen extraction fraction (OEF) and cerebral metabolic rate of oxygen (CMRO₂).

Measurements of these parameters have been performed in the analysis of brain metastases (10), calibrated fMRI (11), or for the effect of acetazolamide administration using ¹⁵O PET (12). However, a limited number of studies have investigated the correlation, particularly the regional correlation, of CVR with other physiological parameters such as OEF and CMRO₂ (13, 14). Previous research (7) has shown a significant association between task-related fMRI responses and underlying physiological factors at rest, such as CVR and baseline venous blood oxygenation (Y_{ν}) . Another study (6) explored similar physiological influences on resting-state fMRI metrics, revealing their significant impact on both resting-state functional activity (RSFA) and functional connectivity (FC) measurements. Additionally, other reports showed a positive correlation between baseline cerebral blood flow (CBF) and CVR, both between- and within-subjects (15–17). Whole brain physiological parameters such as global CBF, global venous oxygenation (Y_v) , RSFA, and CVR have been measured and studied (6, 7). Baseline Y_{ν} was determined in the superior sagittal sinus using the T2-Relaxation-Under-Spin-Tagging (TRUST) technique (8), CVR was measured using inhalation of 5% CO₂ gas, RSFA was eventually obtained, and whole brain baseline cerebral blood flow (CBF) was measured using phase contrast (7). It was shown that the fMRI signal amplitude was positively correlated with CVR and RSFA, but negatively correlated with baseline Y_{ν} . Furthermore, among the physiological modulators themselves, significant correlations were observed between baseline Y_{ν} and baseline CBF, and between CVR and RSFA, suggesting that some of the modulators may partly be of similar physiological origins.

Regional correlations among these physiological parameters may help to elucidate the metabolic demands of different brain areas. Additionally, they may shed light on how these areas respond to changes in blood flow and oxygen supply. In this study, these baseline physiological parameters were measured using MRI covering the full brain. We calculated regional and global correlations between breathing task-derived CVR and baseline CBF, OEF, and CMRO₂ in healthy volunteers and in patients with tumors. Our main objective was to investigate correlations among CVR, CBF, OEF, and CMRO₂ in healthy individuals across lobes of gray matter, as well as to assess their variations between and within subjects. Additionally, we included a small cohort of brain tumor patients to evaluate the feasibility of the method in a clinical setting and to identify potential correlations among individual parameters within the tumor region, as previously described (18).

Methods

Fifteen healthy volunteers (7 female, 8 male, aged 30 ± 5 years) were examined prospectively using a 20-channel head coil on a 3 T scanner (Magnetom Prisma, Siemens Healthineers, Erlangen, Germany). All participants provided written informed consent, and the study was approved by the institutional ethics committee. Additionally, five patients with brain tumors were measured using a 64-channel head coil on the same scanner.

To measure CVR, breath-hold (BH) respiratory challenges were integrated into a standard clinical brain imaging protocol: for block-designed BH tasks, 110 measurements were obtained, which include five and a half BH/FB (free breathing) cycles with 20 measurements (34 s) per full cycle and 10 measurements (17 s) per half cycle. The duration of breath hold time and free breathing time were both 17 s. To measure baseline CBF, a pseudo-continuous arterial spin labeling (pCASL) sequence with 3D gradient- and spin-echo imaging (GRASE) readout was applied before BH tasks. Presaturation before labeling and background suppression during a postlabeling delay (PLD) were added. Baseline OEF was determined based on a gradient-echo sampling of spin-echo (GESSE) pulse sequence (19). The baseline CMRO₂ was then calculated from CBF and OEF. Specific sequence parameters and data analysis are as follows.

CVR (2D gradient-echo EPI): $FOV = 220 \times 220 \times 118 \text{ mm}^3$, matrix size = $64 \times 64 \times 28$, resolution = $3.4 \times 3.4 \times 3.5$ mm³, slice gap = 0.7 mm, in-plane iPAT factor = 2, multiband factor = 2, bandwidth = 1776 Hz/px, TE = 27.08 ms, TR = 1700 ms. Total acquisition time = 3.12 min. Preprocessing including motion correction and slice timing correction was performed with SPM12 (Wellcome Trust Centre for NeuroImaging, UK) and postprocessing was implemented using customized programs written in MATLAB (MathWorks, Natick, MA, USA). In conventional CVR analysis, measurements of end-tidal CO₂ (Et-CO₂) are required and used in a linear regression equation (20). Since we did not have Et-CO₂ measurements available, CVR was estimated by replacing Et-CO₂ with the mean signal of gray matter (21). Motion correction using SPM including realignment and reslicing and nuisance regression was performed to remove the motion corruption induced by the breathholding task.

Baseline CBF (3D pCASL GRASE): FOV = $220 \times 220 \times 120 \text{ mm}^3$ matrix size = $64 \times 64 \times 24$, resolution = $3.4 \times 3.4 \times 5$ mm³, slice and plane partial Fourier = 6/8, slice oversampling = 16.7%, FA = 120° , segments = 2, Bandwidth = 2,298 Hz/px, labeling duration = 1.8 s, PLD = 1.8 s, TE = 17.18 ms, TR = 4,500 ms. This sequence had 20 tag and 20 control volumes and one M_0 volume, for a total scan time of approximately 7 min. CBF was calculated using ASLtbx (22). A labeling efficiency of 0.86 was assumed in the calculation.

Baseline OEF (GESSE): $FOV = 256 \times 192 \times 117 \text{ mm}^3$, partial Fourier = 6/8, matrix size = $128 \times 96 \times 30$, resolution = $2 \times 2 \times 3 \text{ mm}^3$, slice gap = 0.9 mm, TE = 51 ms; TR = 105 ms, number of total echoes = 64, number of echoes before echo center = 20, averages = 3, acquisition time was about 10 min. For OEF analysis, a feedforward ANN (artificial neural network) was used because of its high capability

for nonlinear regression problems (23). Here, an ANN was chosen for its robust curve-fitting, good resilience to noise and outliers, and superior computational speed compared to conventional least-squares regression (LSR) methods. The ANN consisted of a 64-dimensional input layer, two hidden layers (32 and 10-dimensional), and a 4-dimensional output layer. Itwas implemented using the Neural Network Toolbox provided by MATLAB. The ANN was trained based on the full quantitative BOLD (qBOLD) model (24). Thereby, artificial GESSE signals with a known ground truth were simulated for plausible ranges of the input variables S_{SE} , R_{D} , λ , and OEF. To reduce overfitting artifacts, noise was added to the simulated GESSE signals before the actual ANN training (23) was initialized.

T1 weighted anatomical image (T1W): FOV = $230 \times 230 \times 176$ mm3, matrix size = $320 \times 320 \times 176$, resolution = $0.4 \times 0.4 \times 1$ mm3, in-plane iPAT factor = 2, slice partial Fourier = 6/8, TE = 2.63 ms, TR = 1700 ms, TI = 900 ms, FA = 8° , Bandwidth = 2,298 Hz/px, acquisition time was about 5 min.

The CVR and CBF maps were smoothed using a Gaussian kernel with full width at half maximum of 4 mm. Next, all images were coregistered to the T1W and normalized to the Montreal Neurological Institute (MNI) standard brain space for healthy subjects.

Baseline CMRO₂: After smoothing and normalization of CBF and OEF into MNI space, CMRO₂ was calculated as (25):

$$CMRO_2 = CBF \cdot OEF \cdot [H]_a$$
.

The oxygenated heme molar concentration in arterioles $[H]_a$ was assumed to be 7.377 μ mol/mL (24).

Statistical analyses

General linear regression analysis was used to examine the relations between CVR and other parameters in five lobes of gray matter including frontal, parietal, temporal, occipital and insula lobes in individual healthy subjects. Parameter maps were averaged across healthy subjects to compute group-level histograms in the whole brain, gray matter (GM) and white matter (WM). Spearman correlation was performed to check the regional correlations in an Automated Anatomical Labeling (AAL) atlas with 116 indexes. In order to extract the top 12 (i.e., 10% of 116) correlation regions, AASL regions with the lowest *p*-value were selected and plotted. For the patients, tumor regions of interest (ROIs) were manually selected based on the gadolinium contrast enhanced T1 weighted images (CET1W). A correlation matrix was generated to compare voxel-wise Spearman correlations between parameters within these ROIs.

Results

Normalized and averaged maps of CVR, CBF, OEF and CMRO₂ are presented in Figure 1. In the CVR maps, an increased value can be noticed at the location of large draining veins such as the superior sagittal sinus and the transverse sinus. The CBF and CMRO₂ maps demonstrate a similar contrast, although with a different value range. OEF was homogeneous across most of the brain, but not at the center of the brain such as within the thalamus and putamen regions.

After linear regression, a positive correlation between CBF in five lobes and CVR across subjects was found (p < 0.05). Positive correlations between CMRO₂ in the same regions and CVR across subjects were also found (p < 0.05). CBF and CMRO₂ were almost perfectly correlated (p < 0.001, $r^2 = 1.0$). However, correlations between OEF and other parameters were not significant. (p = 0.58 for OEF-CVR, p = 0.15 for OEF-CBF, p = 0.27 for OEF-CMRO₂). Specific results are presented in Figure 2.

The histogram of CVR exhibited two peaks (GM and WM) in the intensity distribution (Figure 3). CBF and CMRO₂ histograms were similarly distributed but showed a wider distribution. However, the histograms of OEF were very different and had a strong peak at the same location (\approx 57.8) both in the whole brain as well as within each of GM and WM separately.

Figure 4 shows the Spearman correlation coefficients r between each pair among CVR, CBF, OEF and CMRO₂. We saw strong positive correlations for CVR vs. OEF and CMRO₂ in the white matter areas, especially for CVR vs. CMRO₂ in the occipital region. On the other hand, some areas showed a strong negative correlation, e.g., CVR vs. OEF in the fronto-insular region or CBF vs. OEF in the insular region. A strong correlation between CBF and CMRO₂ was found in the whole brain except for parts of the frontal region.

The correlations r of top 12 AAL regions with lowest *p*-value are shown in Figure 5. Due to the high correlation between CBF and CMRO₂, all 116 AAL regions were selected (Figure 5E).

The first patient with a brain tumor (melanoma) is presented in Figure 6. The primary tumor was located at the right nuchal. ROI with abnormal CET1W were selected and different parameter maps within this ROI were overlaid. The regions with high CBF showed lower OEF.

The second patient with multiple brain metastases (melanoma) is presented in Figure 7. The metastases were located at gyrus rectus on the left side (first column), in the frontal operculum on the left side (second column and third column), frontal lobe on the right side (fourth column) without CET1W-hyperintersities, and cingulate gyrus on the left side (fifth column). Brain ROIs were masked and different parameter maps within the brain were overlaid on CET1W. The brain ROIs were defined according to CET1W. White matter was not intentionally excluded. Each parameter displayed abnormalities in different locations. OEF showed enhancements at the location with abnormal CET1W. CBF was increased at the first location but decreased at the last location. CVR was decreased in some metastasis locations.

The third patient with brain Glioblastoma is presented in Figure 8. A defect area after resection of a Glioblastoma in the left temporal lobe with infiltration of the adjacent dura could be observed. Brain ROIs were masked and different parameter maps within the brain were overlaid on CET1W. Generally, CBF and CMRO₂ were decreased at the tumor location. CVR was increased at the lower tumor ring, as indicated in the first column.

Voxel-wise Spearman's correlation coefficients between all pairs of physiological parameters in patient tumor ROIs are presented in Supplementary Figure S1. Except the strong correlation between CBF and CMRO₂, there was no correlation between other physiological pairs. The results of the remaining patients are presented in Supplementary Figures S2 and S3. Subject-specific maps of T1W, CVR, CBF and OEF from the first six subjects are presented in Supplementary Figure S4.

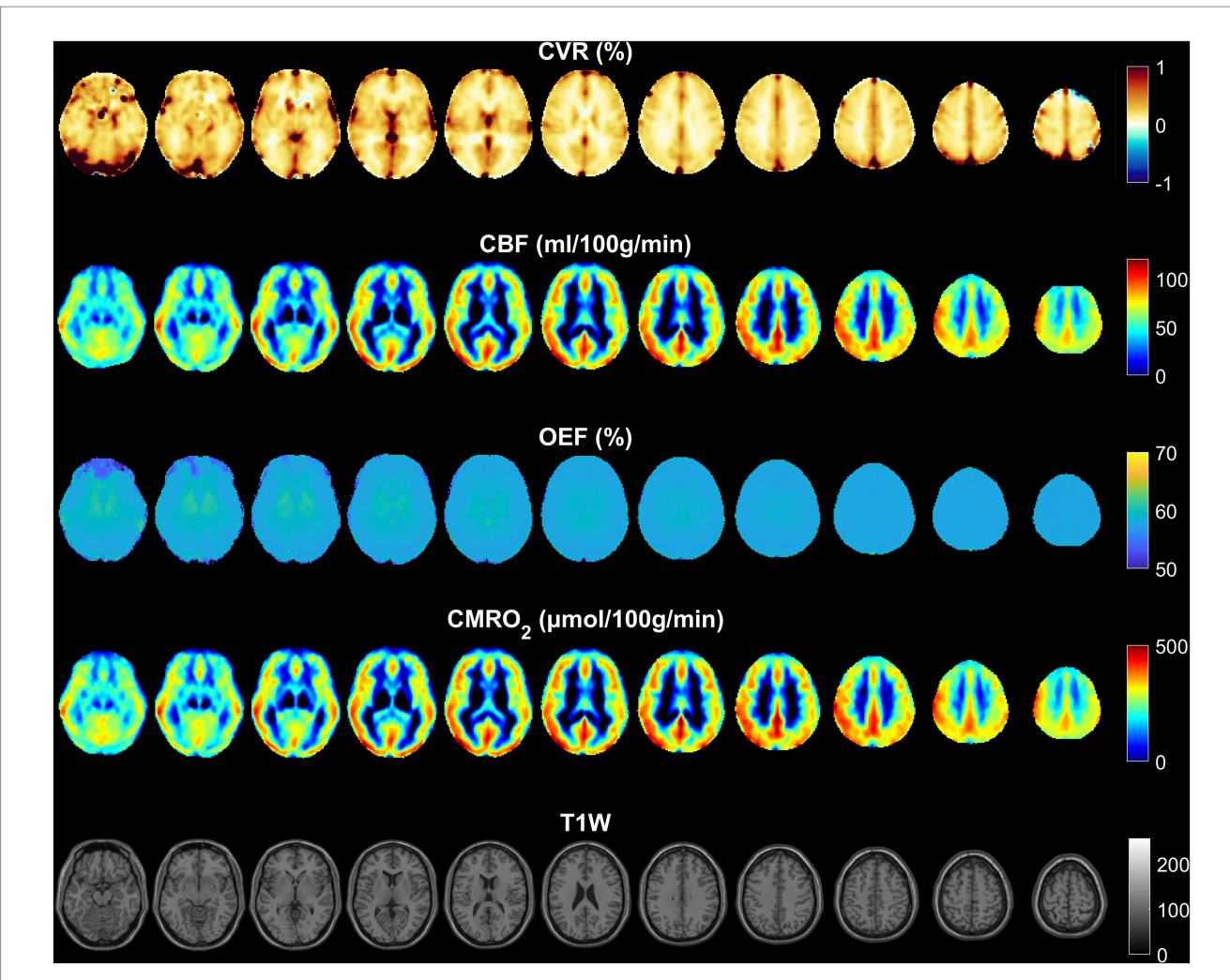


FIGURE 1
Normalized and averaged maps of CVR, CBF, OEF, and $CMRO_2$. The distribution of CBF is similar to $CMRO_2$, since the OEF is very homogeneous. The distribution of CVR is different from CBF and $CMRO_2$, especially in large draining veins.

Discussion

This study aimed to investigate how CVR derived from a breathing task relates to baseline CBF, OEF, and CMRO2. Consistent with previous reports, we found a significant positive correlation between CBF and CVR in five lobes of gray matter (Figure 2A) (6, 15, 17). Additionally, we found no significant correlation between OEF and CBF. This finding contradicts those of earlier research here OEF and CBF was found to be significantly correlated (p = 0.01) (7).

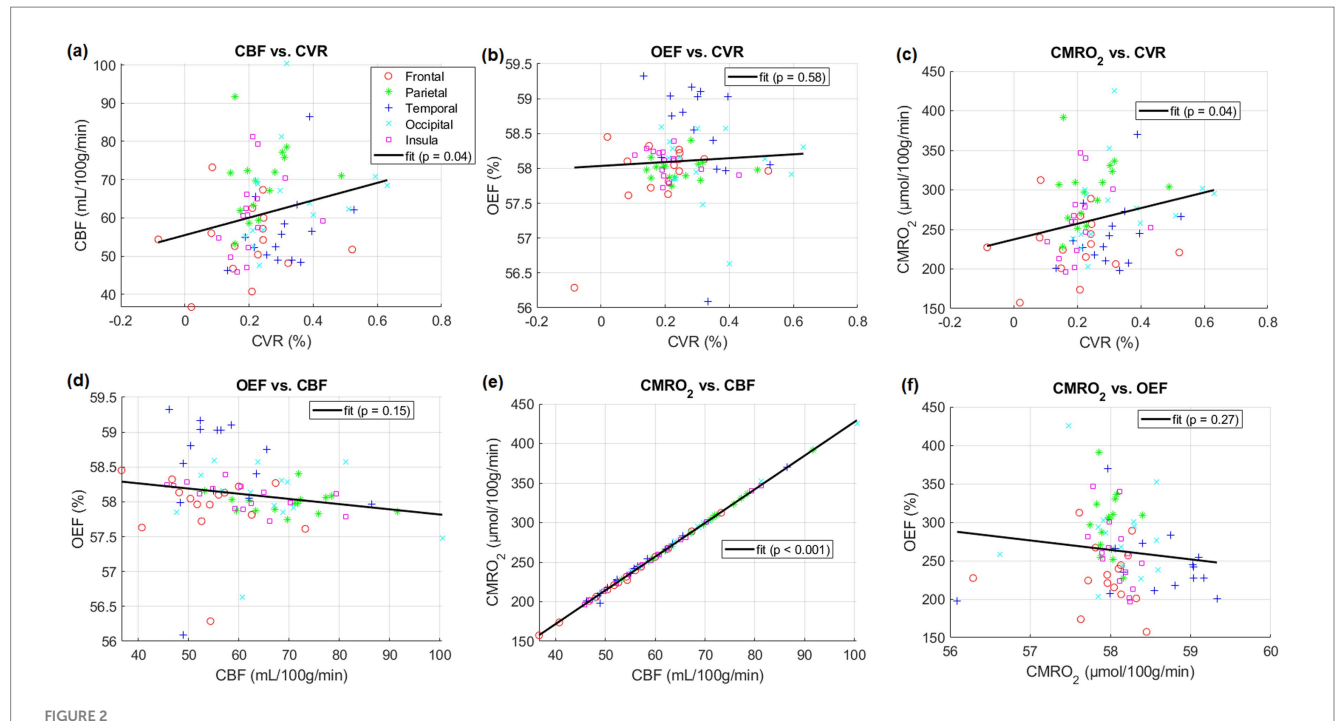
In this study, correlations between OEF and CVR in five lobes were not significant (Figure 2B). Significant positive correlations between CMRO₂ and CVR in these lobes across subjects were also found (Figure 2C).

The CVR maps displayed increased values near the large draining veins, like the superior sagittal and transverse sinuses (Figure 1). These increased values were most likely a result of the interaction between sensitivity of the BOLD signal to blood oxygenation, proximity to large vessels, as well as partial volume effects, and the hemodynamic response in these regions. These elevated values do not necessarily reflect brain tissue reactivity but rather the influence of nearby venous structures. Increased OEF in central brain regions like the thalamus

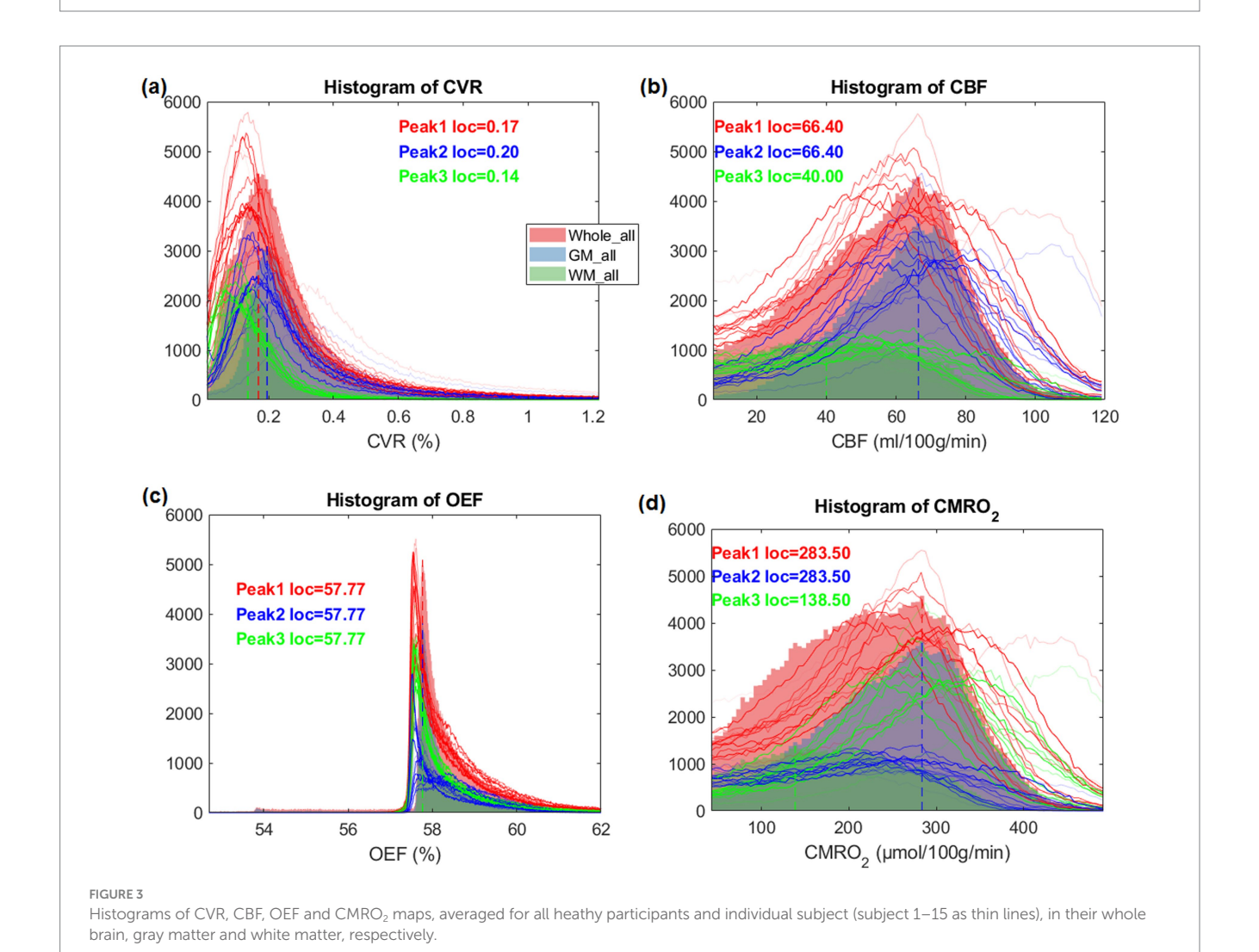
and putamen (Figure 1) may be driven by their high metabolic activity, specialized functions, and unique vascular supply characteristics. These areas have high oxygen demand due to their role in vital processes such as motor control, sensory relay, and synaptic transmission (26). Additionally, the vascular characteristics of these regions—small penetrating arteries and relatively lower blood flow—necessitate higher oxygen extraction to maintain efficient brain function (27, 28).

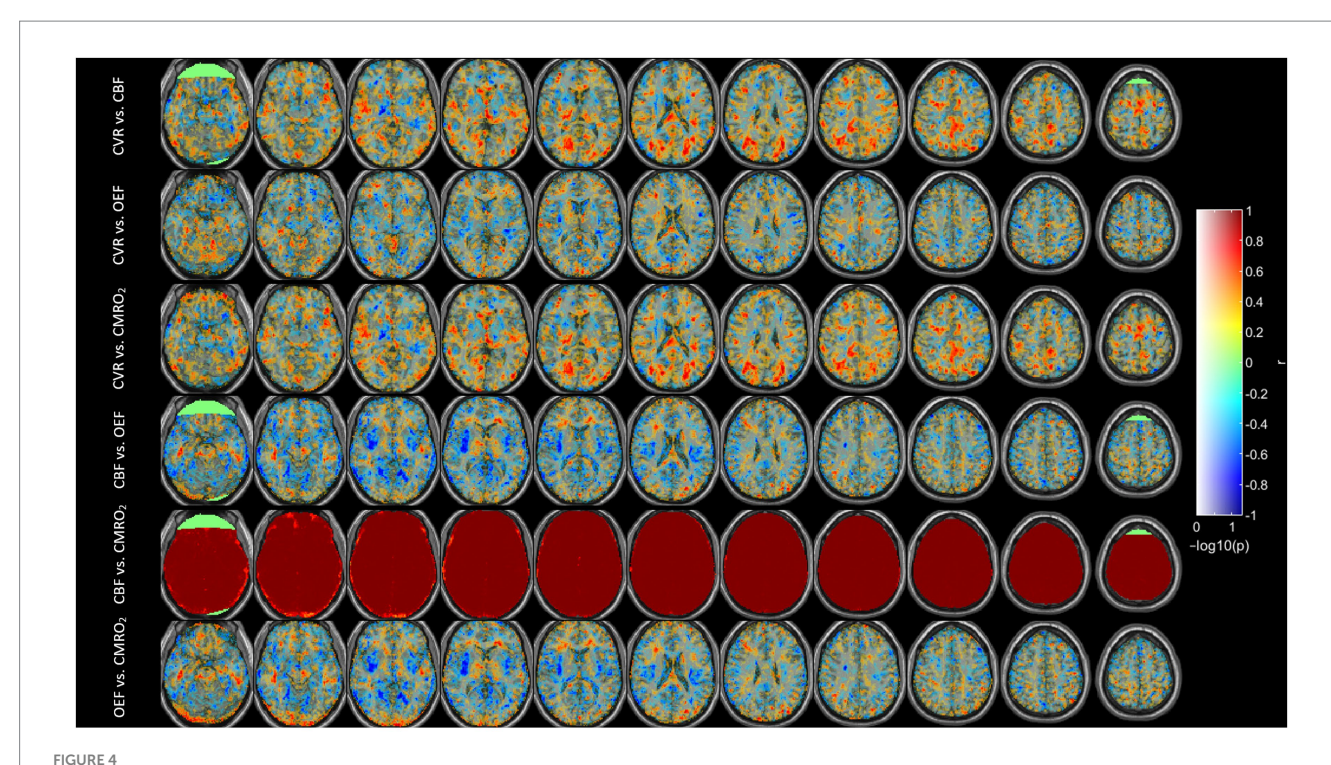
The lower or absence of correlation between OEF and other physiological parameters may arise from the fact that OEF primarily reflects the brain's metabolic demand for oxygen, while other parameters like CBF and CVR are influenced by vascular and hemodynamic factors that do not always correspond directly to metabolic needs. Cerebral autoregulation, regional metabolic variation, and pathological states further contribute to the decoupling of OEF from these other physiological metrics.

The lack of correlation between CBF and OEF in this study, compared to previous studies (13, 14) could arise from measurement technique. Previous studies measured the global OEF in the superior sagittal sinus either using TRUST (14) or susceptometry-based oximetry (13). In global measurement, regional variations in these parameters could be averaged

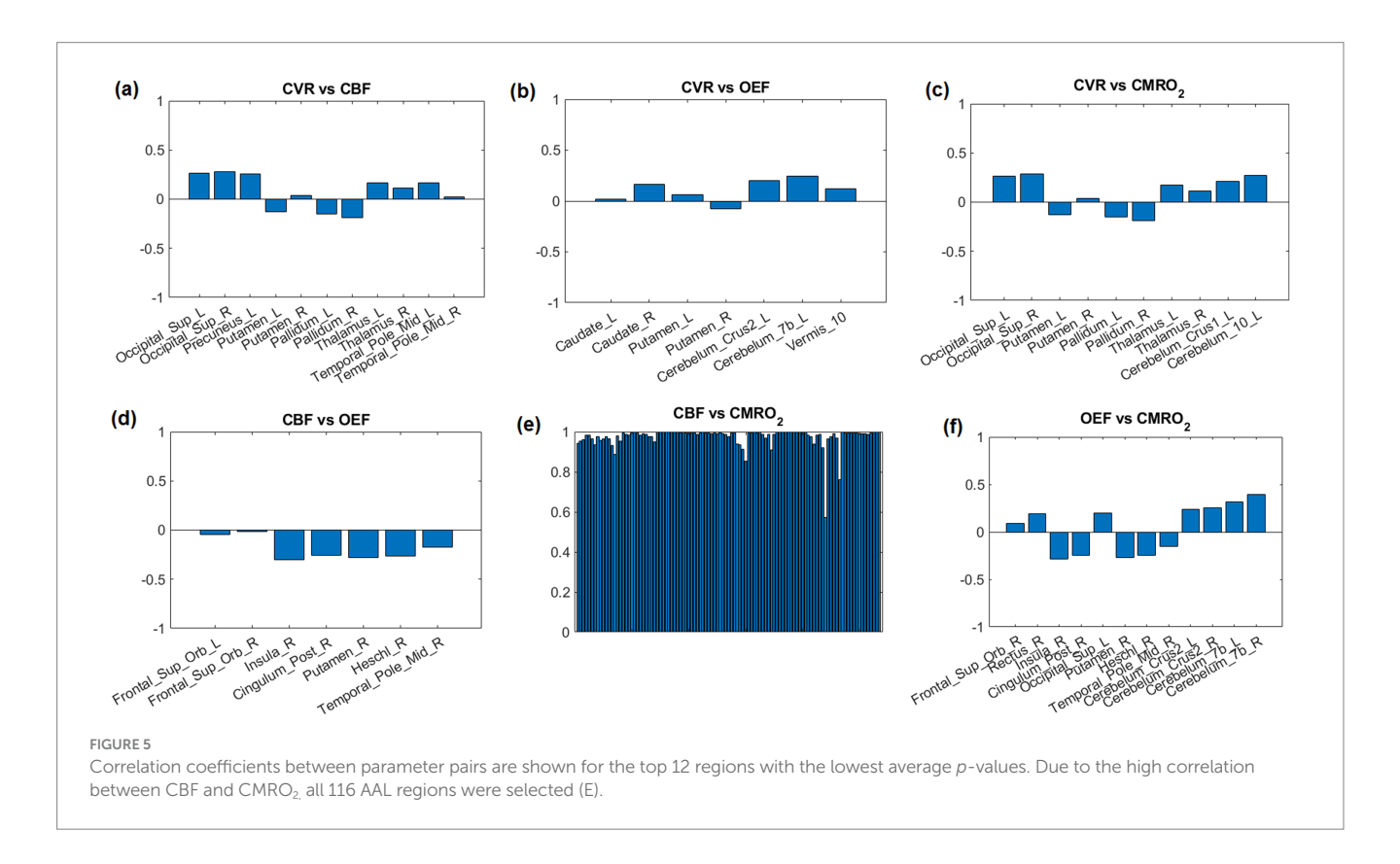


Comparisons between different physiological parameters averaged in listed five lobes of gray matter including frontal, parietal, temporal, occipital and insula lobes of individual subjects, respectively. Linear regressions and their parameters are included.





Correlation coefficients (r) between different parameters across subjects after using Spearman correlation. Correlation coefficients r is mapped to color as shown; $-\log 10(p)$ is mapped to transparency. The range of $-\log 10(p)$ was set to 0-1.3, corresponding to a p-value threshold of p < 0.05.



out, obscuring a relationship that might otherwise be seen in higher-resolution measurements. However according to Figures 1, 4, 5, different brain regions may exhibit varying relationships between CBF and OEF due to differences in metabolic demand. Areas with high baseline metabolism (e.g., the gray matter) could maintain a stable OEF despite

fluctuations in CBF, while regions with lower metabolic demand would show less tight coupling. OEF maps (Figure 1) show relatively homogeneous distributions across much of the cortex, particularly within gray matter, consistent with stable oxygen extraction despite variations in perfusion. However, in subcortical regions such as the thalamus and

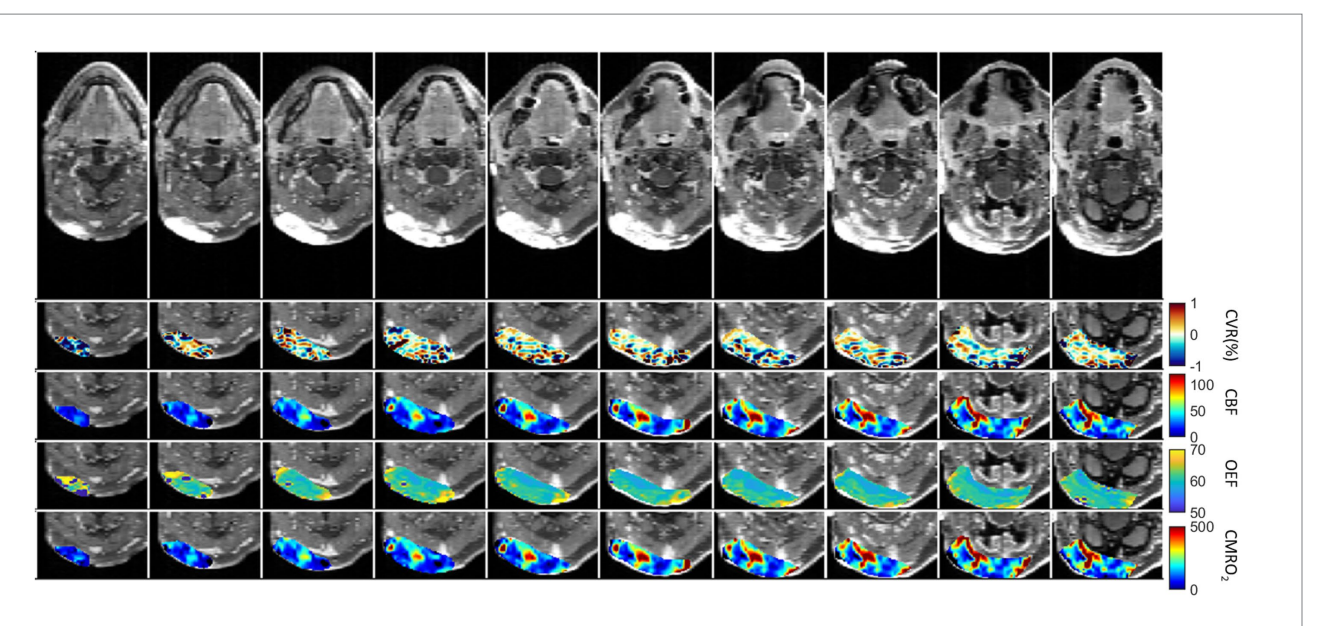


FIGURE 6
First patient with Melanoma (male, 59 years old, after therapy with Encorafenib und Binimetinib). The primary tumor was located at the right nuchal. ROI with abnormal CET1W were selected and different parameter maps within this ROI were overlaid.

putamen, areas known for high metabolic activity, OEF values appear elevated, likely due to increased oxygen demand. In contrast, CBF maps exhibit more spatial variability between gray and white matter regions, and between cortical areas. When these maps are considered alongside the CMRO2 maps (which are derived from CBF \times OEF), it becomes evident that CMRO2 variability is largely driven by CBF fluctuations, since OEF is relatively stable in the cortex. While strong correlations are observed between CBF and CMRO2 across most brain regions (Figure 4), correlations between OEF and either CBF or CMRO2 are weaker or absent, indicating that OEF remains relatively invariant in many areas despite variations in CBF. Figure 5 shows that very few regions met even a liberal p-threshold for significant correlation between OEF and CBF, reinforcing the observation that these parameters are uncoupled across much of the brain.

Except CBF and CMRO₂, averaged maps (Figure 1) and corresponding intensity histograms (Figure 3) of physiological parameters revealed distinct distributions. Comparing to a previous study (29), the peak location of CVR in this study (0.17) is very similar. The histograms of CBF and CMRO2 were similarly distributed but showed a broader range. The peak location of CBF is around 65 mL/100 g/min which is close to the result of a previous study (30). However, the histograms of OEF were very different and had a strong peak at the same location in the whole brain as well as within each of GM and WM separately. Accordingly, we subsequently investigated the regional correlations between them.

CBF and CMRO₂ are significantly correlated (Figure 4). This phenomenon is easily understandable since OEF is very homogenous and CMRO₂ is the product of CBF and OEF. Therefore, CBF and CMRO₂ are similarly distributed. The regional correlations between CVR, OEF, CBF, and CMRO₂ highlight the regional variability in how the brain regulates its blood supply and oxygen metabolism. Strong positive correlations in the white matter and occipital region suggest efficient matching of blood flow and oxygen metabolism, while negative correlations in areas like the insular region reveal

compensatory mechanisms where blood flow and oxygen extraction are inversely related. In fMRI studies of visual stimulation (31), occipital regions showed coordinated increases in CBF, BOLD, and CMRO₂ response. An inverse correlation of white matter CBF with connectivity has also been shown previously (32).

For regional correlations we selected the 12 AAL regions with the most significant correlations according to the lowest averaged *p*-value in each region (Figure 5). These regions could also be noticed in Figure 4.

Comparing to TRUST (8) we could measure full brain covered OEF with only minimal artifacts. The GESSE pulse sequence is a sequence that allows a hybrid mapping of T₂ and T₂* relaxation times. It was developed to separate macroscopic and microscopic magnetic field inhomogeneities in MRI in microstructural brain imaging (18). In GESSE, a set of gradient echoes (GREs) are embedded around the spin echo (SE) of a single SE sequence (24). This sequence structure allows a simultaneous acquisition of a set of images corresponding to different GRE times (TEs) and therefore allows simultaneous T₂ and T_2^* mapping. The measurement of T_2 and T_2^* using GESSE was developed and applied for OEF mapping (23-25). GESSE is insensitive to RF pulse errors and does not suffer from significant field distortions, therefore providing a robust mapping technique in cerebral imaging. The range of OEF measured by qBOLD MRI typically lies between 0.2 and 0.5 (or 20-50%) under healthy physiological conditions (24). According to the histogram of OEF (Figure 3) the peak location is about 57.77 which is very close to the one in the literature (24).

In pathological conditions, the ability of blood vessels to widen in response to a stimulus may be compromised due to an already widened baseline, as seen in sickle cell disease where cerebral blood flow (CBF) is elevated and cerebrovascular reactivity (CVR) diminished (33, 34). In diseases characterized by narrowing or blockage of vessels, such as steno-occlusive diseases, a vasodilatory stimulus can increase CBF in regions with robust vasodilatory capacity. However, this may unexpectedly decrease CBF in neighboring areas with preserved or limited vasodilatory

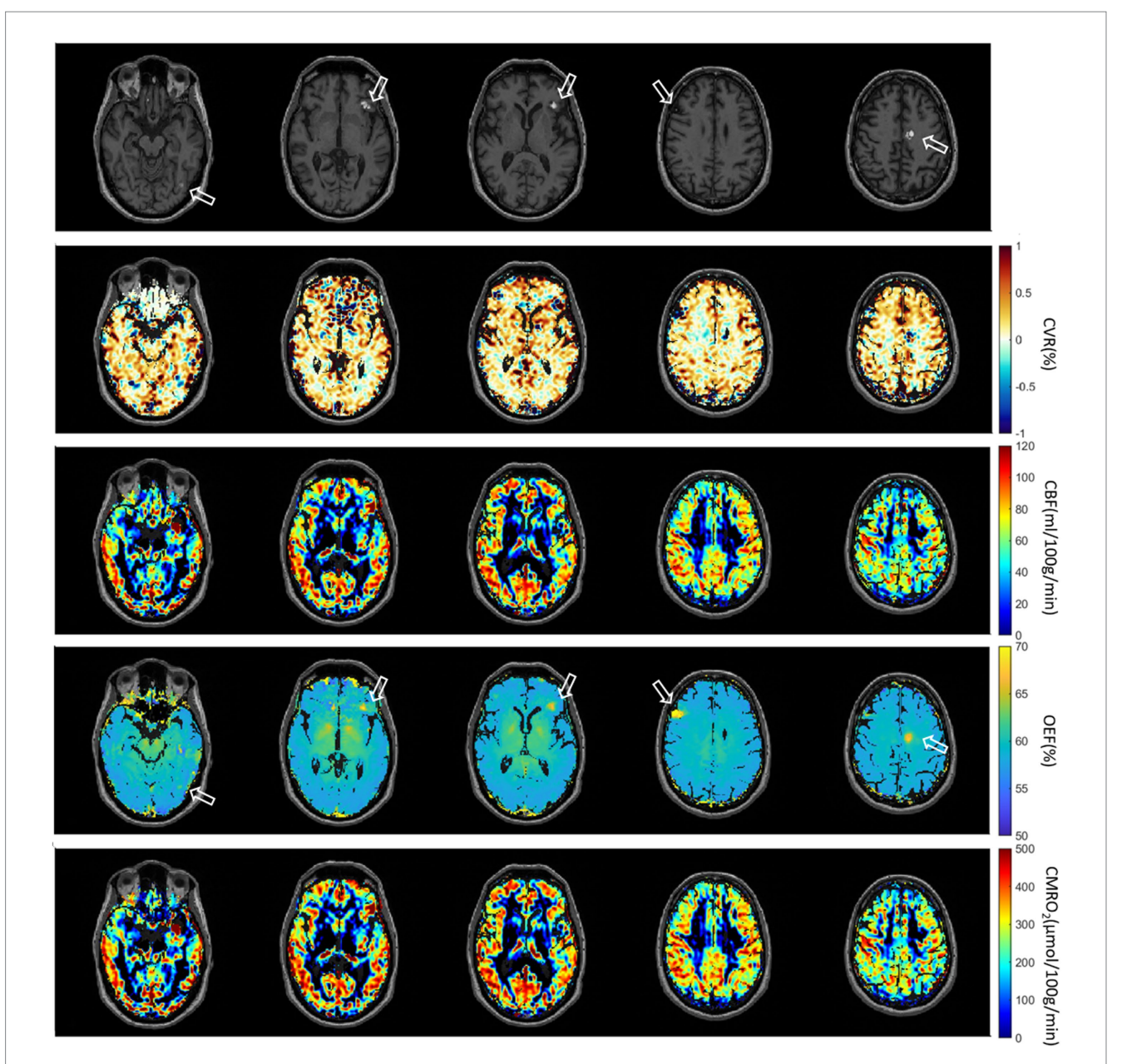


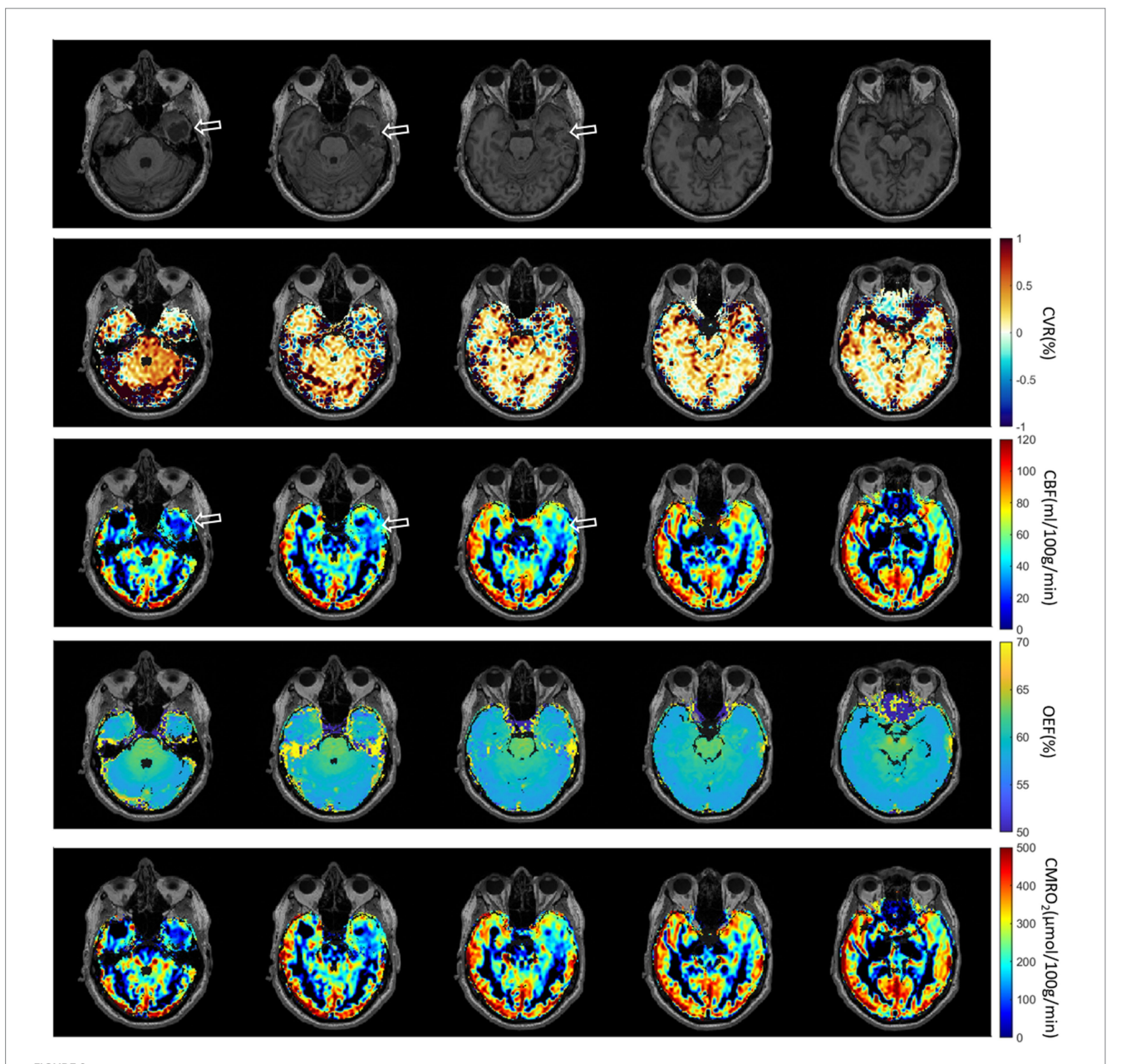
FIGURE 7
Second patient with Melanoma (male, 55 years old, after therapy with Nivolumab). The metastases are located at gyrus rectus on the left side (first column), in the frontal operculum on the left side (second column and third column), frontal lobe on the right side (fourth column) without CET1W-hyperintersities, and cingulate gyrus on the left side (fifth column).

capacity (35). This phenomenon, known as "vascular steal," may result in apparent negative CVR responses, either with or without changes in CBF (35). The relationship between CBF and CVR in pathological cases is often complex and not easily discernible. Similar to this principle, physiological parameters are distributed differently in the brain tumor cases (Figures 6–8). Except the strong correlation between CBF and CMRO₂, there was no correlation between other physiological parameters (Supplementary Figure S1). Due to the differences between physiological parameters, complete measurements of all of them will help the physician to discover different aspect of tumor properties. These metrics help physicians understand critical tumor characteristics such as vascularity, metabolic demand, hypoxia, aggressiveness, and response to treatment. By integrating these data, clinicians can develop more personalized and

effective treatment plans, optimize therapeutic strategies, and improve prognosis assessment for patients with brain tumors.

We found that, except for CBF and CMRO2, no other parameters were correlated in tumor cases. This indicated that, apart from the fact that the small cohort of tumor patients may not permit a rigorous statistical analysis and interpretation, (i) local tumor blood flow is correlated with metabolic demand for both tumor and healthy brain regions, as already demonstrated in previous works (36, 37), and (ii) that cerebrovascular reactivity appears independent from other physiological parameters in the tumor region, suggesting a perturbed vascular architecture (38).

There are several limitations of this study. First, GESSE is a very long measurement that takes about 10 min. The versatility of



Third patient with brain Glioblastoma (male, 67 years old, after resection). The defect area after resection of a Glioblastoma in the left temporal lobe with infiltration of the adjacent dura could be observed.

combined GE and SE methodology has been demonstrated in various approaches, based on a wide range of sequence implementations, and differing in the readout (single- or multiple-line acquisitions), spatial resolution, number and type of echoes used (39). EPI outperforms single-line acquisitions in terms of acquisition time (TA) and temporal resolution, making it the current method of choice for fast imaging sequences. However, EPI suffers from distortion, blurring, and local signal loss (40). Secondly, CVR is measured with a breath-holding task. This task requires notable cooperation of patients or volunteers. Without gas challenges, CVR can also be measured during resting-state (41–43). However, special care needs to be taken for it to be more reliable (3, 16). The efficiency of breath-holding as a method for inducing

hypercapnia needs to be correlated with physiological measurements like SPO₂ and blood CO₂ levels to ensure adequacy. Without monitoring these, the induced hypercapnia may be inconsistent or inadequate, leading to potential bias in the measurement of CVR and other related parameters. This could undermine the reliability of the test results, highlighting the need for better understanding and standardization in CVR testing. While breath-holding is commonly used to assess CVR, its associated hemodynamic changes (like reduced venous return, altered cardiac output, and blood pressure fluctuations) can influence the results. These changes are sometimes monitored, but often they are not fully accounted for, which may introduce bias into the assessment of CVR parameters. To improve accuracy, more careful monitoring and control of these

hemodynamic factors such as lagged-GLM¹⁷ for optimization are needed during CVR testing (44) and calculation. Thirdly, the ASL scan was a single PLD 3D pCASL. This sequence was not optimized for voxel-wise CBF measures in white matter (45). Finally, by using a constant $[H]_a$ in the CMRO₂ equation, both the natural variance of and differences in hematocrit between biological sexes is neglected. This may significantly change the oxygenated heme molar concentration in arterioles. Additionally, the chemotherapy treatment in a participant with a metastatic brain could also significantly alter hematocrit.

Conclusion

This study demonstrates a significant positive correlation between CVR and baseline CBF in five lobes of gray matter, indicating a close relationship between vascular reactivity and resting perfusion. In contrast, the weak or absent correlations between OEF and other parameters suggest that OEF reflects distinct metabolic processes less directly coupled to vascular dynamics. The observed regional variability in the relationships among CVR, CBF, OEF, and CMRO₂ highlights the heterogeneous nature of cerebral hemodynamics and oxygen metabolism.

Data availability statement

The data analyzed in this study is subject to the following licenses/ restrictions: The data that support the findings of this study are available from the corresponding author upon reasonable request. Requests to access these datasets should be directed to ke.zhang@uni-heidelberg.de.

Ethics statement

The studies involving humans were approved by Medical faculty of Heidelberg University. The studies were conducted in accordance with the local legislation and institutional requirements. The participants provided their written informed consent to participate in this study. Written informed consent was obtained from the individual(s) for the publication of any potentially identifiable images or data included in this article.

Author contributions

KZ: Conceptualization, Data curation, Formal analysis, Funding acquisition, Investigation, Methodology, Project administration, Software, Supervision, Validation, Visualization, Writing – original draft, Writing – review & editing. ST: Methodology, Writing – review & editing. MW: Writing – review & editing. JJ: Data curation, Writing – review & editing. ES: Writing – review & editing. CZ: Data curation, Writing – review & editing. ML: Resources, Writing – review & editing. H-UK: Resources, Writing – review & editing. OS: Data curation, Writing – review & editing. FK: Data curation, Funding acquisition, Writing – review & editing.

Funding

The author(s) declare that no financial support was received for the research and/or publication of this article.

Conflict of interest

The authors declare that the research was conducted in the absence of any commercial or financial relationships that could be construed as a potential conflict of interest.

The handling editor IR declared a past co-authorship https://link. springer.com/article/10.1007/s12021-024-09703-4 with the author ML.

The author(s) declared that they were an editorial board member of Frontiers, at the time of submission. This had no impact on the peer review process and the final decision.

Generative AI statement

The authors declare that no Gen AI was used in the creation of this manuscript.

Any alternative text (alt text) provided alongside figures in this article has been generated by Frontiers with the support of artificial intelligence and reasonable efforts have been made to ensure accuracy, including review by the authors wherever possible. If you identify any issues, please contact us.

Publisher's note

All claims expressed in this article are solely those of the authors and do not necessarily represent those of their affiliated organizations, or those of the publisher, the editors and the reviewers. Any product that may be evaluated in this article, or claim that may be made by its manufacturer, is not guaranteed or endorsed by the publisher.

Supplementary material

The Supplementary material for this article can be found online at: https://www.frontiersin.org/articles/10.3389/fneur.2025.1534844/full#supplementary-material

SUPPLEMENTARY FIGURE S1

Voxel-wise Spearman's correlation coefficients between all pairs of physiological parameters in the tumor ROIs from patient 1 (a), patient 2 (b) and patient 3 (c).

SUPPLEMENTARY FIGURE S2

Fourth patient with metastatic Melanoma (male, 67 years old, after radiotherapy).

SUPPLEMENTARY FIGURE S3

Fifth patient with metastatic Melanoma (male, 40 years old, after radiotherapy).

SUPPLEMENTARY FIGURE S4

Individual T1 weighted anatomical, CVR, CBF and OEF maps were calculated in all subjects (left-right).

SUPPLEMENTARY FIGURE S5

Breath-holding task design—five blocks, each consisting of 10 repetition of free breathing (FB), 10 repetition of breath-hold (BH), TR is equal to 1.7s.

References

- 1. Sleight E, Stringer MS, Marshall I, Wardlaw JM, Thrippleton MJ. Cerebrovascular reactivity measurement using magnetic resonance imaging: a systematic review. *Front Physiol.* (2021) 12:643468. doi: 10.3389/fphys.2021.643468
- 2. Fisher JA, Venkatraghavan L, Mikulis DJ. Magnetic resonance imaging-based cerebrovascular reactivity and hemodynamic reserve. *Stroke*. (2018) 49:2011–8. doi: 10.1161/STROKEAHA.118.021012
- 3. Liu P, Xu C, Lin Z, Sur S, Li Y, Yasar S, et al. Cerebrovascular reactivity mapping using intermittent breath modulation. *NeuroImage*. (2020) 215:116787. doi: 10.1016/j.neuroimage.2020.116787
- 4. Griffeth VE, Perthen JE, Buxton RB. Prospects for quantitative fMRI: investigating the effects of caffeine on baseline oxygen metabolism and the response to a visual stimulus in humans. *NeuroImage*. (2011) 57:809–16. doi: 10.1016/j.neuroimage.2011.04.064
- 5. Kim SG, Ogawa S. Biophysical and physiological origins of blood oxygenation level-dependent fMRI signals. *J Cereb Blood Flow Metab.* (2012) 32:1188–206. doi: 10.1038/jcbfm.2012.23
- 6. Chu PPW, Golestani AM, Kwinta JB, Khatamian YB, Chen JJ. Characterizing the modulation of resting-state fMRI metrics by baseline physiology. *NeuroImage*. (2018) 173:72–87. doi: 10.1016/j.neuroimage.2018.02.004
- 7. Liu P, Hebrank AC, Rodrigue KM, Kennedy KM, Park DC, Lu H. A comparison of physiologic modulators of fMRI signals. *Hum Brain Mapp*. (2013) 34:2078–88. doi: 10.1002/hbm.22053
- 8. Lu H, Ge Y. Quantitative evaluation of oxygenation in venous vessels using T2-relaxation-under-spin-tagging MRI. *Magn Reson Med.* (2008) 60:357–63. doi: 10.1002/mrm.21627
- 9. Xu F, Li W, Liu P, Hua J, Strouse JJ, Pekar JJ, et al. Accounting for the role of hematocrit in between-subject variations of MRI-derived baseline cerebral hemodynamic parameters and functional BOLD responses. *Hum Brain Mapp.* (2018) 39:344–53. doi: 10.1002/hbm.23846
- 10. van Grinsven EE, de Leeuw J, Siero JCW, JJC V, MJE v Z, Cho J, et al. Evaluating physiological MRI parameters in patients with brain metastases undergoing stereotactic radiosurgery-a preliminary analysis and case report. *Cancers* (Basel). (2023) 15:15. doi: 10.3390/cancers15174298
- 11. Germuska M, Chandler HL, Stickland RC, Foster C, Fasano F, Okell TW, et al. Dual-calibrated fMRI measurement of absolute cerebral metabolic rate of oxygen consumption and effective oxygen diffusivity. *NeuroImage*. (2019) 184:717–28. doi: 10.1016/j.neuroimage.2018.09.035
- 12. Watabe T, Shimosegawa E, Kato H, Isohashi K, Ishibashi M, Tatsumi M, et al. Paradoxical reduction of cerebral blood flow after acetazolamide loading: a hemodynamic and metabolic study with (15)O PET. *Neurosci Bull.* (2014) 30:845–56. doi: 10.1007/s12264-013-1459-z
- 13. Jain V, Langham MC, Wehrli FW. MRI estimation of global brain oxygen consumption rate. *J Cereb Blood Flow Metab*. (2010) 30:1598–607. doi: 10.1038/jcbfm.2010.49
- 14. Xu F, Ge Y, Lu H. Noninvasive quantification of whole-brain cerebral metabolic rate of oxygen (CMRO2) by MRI. *Magn Reson Med.* (2009) 62:141–8. doi: 10.1002/mrm.21994
- 15. Leoni RF, Oliveira IA, Pontes-Neto OM, Santos AC, Leite JP. Cerebral blood flow and vasoreactivity in aging: an arterial spin labeling study. *Braz J Med Biol Res.* (2017) 50:e5670. doi: 10.1590/1414-431X20175670
- 16. Stickland RC, Zvolanek KM, Moia S, Ayyagari A, Caballero-Gaudes C, Bright MG. A practical modification to a resting state fMRI protocol for improved characterization of cerebrovascular function. *NeuroImage*. (2021) 239:118306. doi: 10.1016/j.neuroimage.2021.118306
- 17. Stickland RC, Zvolanek KM, Moia S, Caballero-Gaudes C, Bright MG. Lagoptimized blood oxygenation level dependent cerebrovascular reactivity estimates derived from breathing task data have a stronger relationship with baseline cerebral blood flow. *Front Neurosci.* (2022) 16:910025. doi: 10.3389/fnins.2022.910025
- 18. Pillai JJ, Zaca D. Clinical utility of cerebrovascular reactivity mapping in patients with low grade gliomas. *World J Clin Oncol.* (2011) 2:397–403. doi: 10.5306/wjco.v2.i12.397
- 19. Yablonskiy DA, Haacke EM. An MRI method for measuring T2 in the presence of static and RF magnetic field inhomogeneities. *Magn Reson Med.* (1997) 37:872–6. doi: 10.1002/mrm.1910370611
- 20. Liu P, De Vis JB, Lu H. Cerebrovascular reactivity (CVR) MRI with CO2 challenge: a technical review. NeuroImage. (2019) 187:104–15. doi: 10.1016/j.neuroimage.2018.03.047
- 21. Bright MG, Murphy K. Reliable quantification of BOLD fMRI cerebrovascular reactivity despite poor breath-hold performance. NeuroImage. (2013) 83:559–68. doi: 10.1016/j.neuroimage.2013.07.007
- 22. Wang Z, Aguirre GK, Rao H, Wang J, Fernández-Seara MA, Childress AR, et al. Empirical optimization of ASL data analysis using an ASL data processing toolbox: ASLtbx. *Magn Reson Imaging*. (2008) 26:261–9. doi: 10.1016/j.mri.2007.07.003

- 23. Domsch S, Murle B, Weingartner S. Oxygen extraction fraction mapping at 3 tesla using an artificial neural network: a feasibility study. *Magn Reson Med.* (2018) 79:890–9. doi: 10.1002/mrm.26749
- 24. He X, Yablonskiy DA. Quantitative BOLD: mapping of human cerebral deoxygenated blood volume and oxygen extraction fraction: default state. *Magn Reson Med.* (2007) 57:115–26. doi: 10.1002/mrm.21108
- 25. Hubertus S, Thomas S, Cho J, Zhang S, Wang Y, Schad LR. Comparison of gradient echo and gradient echo sampling of spin echo sequence for the quantification of the oxygen extraction fraction from a combined quantitative susceptibility mapping and quantitative BOLD (QSM+qBOLD) approach. *Magn Reson Med.* (2019) 82:1491–503. doi: 10.1002/mrm.27804
- 26. Van Cauter S, Severino M, Ammendola R. Bilateral lesions of the basal ganglia and thalami (central grey matter)-pictorial review. *Neuroradiology*. (2020) 62:1565–605. doi: 10.1007/s00234-020-02511-v
- 27. Ito H, Ibaraki M, Yamakuni R, Hakozaki M, Ukon N, Ishii S, et al. Oxygen extraction fraction is not uniform in human brain: a positron emission tomography study. *J Physiol Sci.* (2023) 73:25. doi: 10.1186/s12576-023-00880-6
- 28. Yang L, Cho J, Chen T, Gillen KM, Li J, Zhang Q, et al. Oxygen extraction fraction (OEF) assesses cerebral oxygen metabolism of deep gray matter in patients with pre-eclampsia. Eur Radiol. (2022) 32:6058–69. doi: 10.1007/s00330-022-08713-7
- 29. Hou XR, Liu PY, Li Y, Jiang D, De Vis JB, Lin Z, et al. The association between BOLD-based cerebrovascular reactivity (CVR) and end-tidal CO2 in healthy subjects. NeuroImage. (2020) 207:116365. doi: 10.1016/j.neuroimage.2019.116365
- 30. Garrett DD, Lindenberger U, Hoge RD, Gauthier CJ. Age differences in brain signal variability are robust to multiple vascular controls. *Sci Rep.* (2017) 7:10149. doi: 10.1038/s41598-017-09752-7
- 31. Hubbard NA, Turner MP, Ouyang M, Himes L, Thomas BP, Hutchison JL, et al. Calibrated imaging reveals altered grey matter metabolism related to white matter microstructure and symptom severity in multiple sclerosis. *Hum Brain Mapp.* (2017) 38:5375–90. doi: 10.1002/hbm.23727
- 32. Aslan S, Huang H, Uh J, Mishra V, Xiao G, van Osch MJP, et al. White matter cerebral blood flow is inversely correlated with structural and functional connectivity in the human brain. *NeuroImage*. (2011) 56:1145–53. doi: 10.1016/j.neuroimage.2011.02.082
- 33. Kosinski PD, Croal PL, Leung J, Williams S, Odame I, GMT H, et al. The severity of anaemia depletes cerebrovascular dilatory reserve in children with sickle cell disease: a quantitative magnetic resonance imaging study. *Br J Haematol.* (2017) 176:280–7. doi: 10.1111/bjh.14424
- 34. Vaclavu L, Meynart BN, Mutsaerts H, Petersen ET, Majoie CBLM, VanBavel ET, et al. Hemodynamic provocation with acetazolamide shows impaired cerebrovascular reserve in adults with sickle cell disease. *Haematologica*. (2019) 104:690–9. doi: 10.3324/haematol.2018.206094
- 35. Sobczyk O, Battisti-Charbonney A, Fierstra J, Mandell DM, Poublanc J, Crawley AP, et al. A conceptual model for CO(2)-induced redistribution of cerebral blood flow with experimental confirmation using BOLD MRI. *NeuroImage*. (2014) 92:56–68. doi: 10.1016/j.neuroimage.2014.01.051
- 36. Bonekamp D, Mouridsen K, Radbruch A, Kurz FT, Eidel O, Wick A, et al. Assessment of tumor oxygenation and its impact on treatment response in bevacizumabtreated recurrent glioblastoma. *J Cereb Blood Flow Metab.* (2017) 37:485–94. doi: 10.1177/0271678X16630322
- 37. Madsen SS, Lindberg U, Asghar S, Olsen KS, Møller K, HBW L, et al. Reproducibility of cerebral blood flow, oxygen metabolism, and lactate and N-acetyl-aspartate concentrations measured using magnetic resonance imaging and spectroscopy. *Front Physiol.* (2023) 14:3352. doi: 10.3389/fphys.2023.1213352
- 38. Breckwoldt MO, Bode J, Sahm F, Krüwel T, Solecki G, Hahn A, et al. Correlated MRI and ultramicroscopy (MR-UM) of brain tumors reveals vast heterogeneity of tumor infiltration and neoangiogenesis in preclinical models and human disease. *Front Neurosci.* (2019) 12:1004. doi: 10.3389/fnins.2018.01004
- 39. Kuppers F, Yun SD, Shah NJ. Development of a novel 10-echo multi-contrast sequence based on EPIK to deliver simultaneous quantification of T(2) and T(2)(*) with application to oxygen extraction fraction. $Magn\ Reson\ Med.\ (2022)\ 88:1608-23.$ doi: 10.1002/mrm.29305
- 40. Embleton KV, Haroon HA, Morris DM, MAL R, GJM P. Distortion correction for diffusion-weighted MRI tractography and fMRI in the temporal lobes. $\it Hum\ Brain\ Mapp.\ (2010)\ 31:1570-87.\ doi: 10.1002/hbm.20959$
- 41. Golestani AM, Wei LL, Chen JJ. Quantitative mapping of cerebrovascular reactivity using resting-state BOLD fMRI: validation in healthy adults. *NeuroImage*. (2016) 138:147–63. doi: 10.1016/j.neuroimage.2016.05.025
- 42. Jahanian H, Christen T, Moseley ME, Pajewski NM, Wright CB, Tamura MK, et al. Measuring vascular reactivity with resting-state blood oxygenation level-dependent (BOLD) signal fluctuations: a potential alternative to the breath-holding challenge? *J Cereb Blood Flow Metab.* (2017) 37:2526–38. doi: 10.1177/0271678X16670921

- 43. Liu P, Li Y, Pinho M, Park DC, Welch BG, Lu H. Cerebrovascular reactivity mapping without gas challenges. *NeuroImage*. (2017) 146:320–6. doi: 10.1016/j.neuroimage.2016.11.054
- 44. Zvolanek KM, Moia S, Dean JN, Stickland RC, Caballero-Gaudes C, Bright MG. Comparing end-tidal CO(2), respiration volume per time (RVT), and average gray matter signal for mapping cerebrovascular reactivity amplitude and delay with breath-
- hold task BOLD fMRI. *NeuroImage*. (2023) 272:120038. doi: 10.1016/j.neuroimage.2023.120038
- 45. Skurdal MJ, Bjornerud A, van Osch MJ, Nordhøy W, Lagopoulos J, Groote IR. Voxel-wise perfusion assessment in cerebral white matter with PCASL at 3T; is it possible and how long does it take? *PLoS One.* (2015) 10:e0135596. doi: 10.1371/journal.pone.0135596